Fabrication and Characterization of a Sialoside-Based Carbohydrate Microarray Biointerface for Protein Binding Analysis with Surface Plasmon Resonance Imaging

Matthew J. Linman,[†] Hai Yu,[‡] Xi Chen,[‡] and Quan Cheng*[,†]

Department of Chemistry, University of California, Riverside, California 92521, and Department of Chemistry, University of California, Davis, California 95616

ABSTRACT Monitoring multiple biological interactions in a multiplexed array format has numerous advantages. However, converting well-developed surface chemistry for spectroscopic measurements to array-based high-throughput screening is not a trivial process and often proves to be the bottleneck in method development. This paper reports the fabrication and characterization of a new carbohydrate microarray with synthetic sialosides for surface plasmon resonance imaging (SPRi) analysis of lectin-carbohydrate interactions. Contact printing of functional sialosides on neutravidin-coated surfaces was carried out and the properties of the resulting elements were characterized by fluorescence microscopy and atomic force microscopy (AFM). *Sambucus nigra* agglutinin (SNA) was deposited on four different carbohydrate functionalized surfaces and differential binding was analyzed to reveal affinity variation as a function of headgroup sialic acid structures and linking bonds. SPRi studies indicated that this immobilization method could result in high quality arrays with RSD < 5% from array element to array element, superior to the conventional covalent linkage used for protein cholera toxin (CT) in a comparison experiment, which yields nonuniform array elements with RSD > 15%. Multiplexed detection of SNA/biotinylated sialoside interactions on arrays up to 400 elements has been performed with good data correlation, demonstrating the effectiveness of the biotin−neutravidin-based biointerface to control probe orientation for reproducible and efficient protein binding to take place. Additionally, the regeneration of the array surface was demonstrated with a glycine stripping buffer, rendering this interface reusable. This in-depth study of array surface chemistry offers useful insight into experimental conditions that can be optimized for better performance, allowing many different protein-based biointeractions to be monitored in a similar manner.

KEYWORDS: carbohydrate microarray • surface plasmon resonance imaging • biotinylated sialosides • biointerface • biosensor

INTRODUCTION

Carbohydrates are key components in cell surface interactions with both proteins and lipids, responsible for recognition, adhesion, and cell-to-cell signaling (1). Since they are structurally complex, there has been considerable effort in synthesizing carbohydrate analogs and investigating their structure−function properties. Monitoring multiple carbohydrate interactions is challenging but highly desirable for gaining affinity information in a timely and cost-effective manner, particularly for pharmaceutical research. This has led to the construction of carbohydrate microarrays for multiplexed detection of protein-carbohydrate interactions as early as in 2002 (2−5). Since then there have been a number of reports on carbohydrate microarrays, and the subject has been the topic for several reviews in the past few years (6−11).

Several commercial instruments are available for fabrication of microarrays with varied quality. The methods for array fabrication can generally be classified as either contact or noncontact printing. The former utilizes pin-type arrayers that transfer a defined volume of sample by directly touching the surface of the substrate, whereas the latter dispenses the sample droplets onto the substrate without a direct contact to the surface. The most common noncontact printing methods are photolithography and inkjet printing. Photolithography is very useful to pattern a variety of materials with different surface chemistries (12). However, it is incompatible with photosensitive compounds, including many biomolecules that cannot be deposited onto photoresists or metals. Inkjet printing, while cheaper than their contact printing counterparts, suffers from multiple drawbacks such as unsuitability to print on glass slides (13) and droplet smearing (14). Contact printing has been widely used and many pin-type arrayers are available, which are usually simpler in design, less expensive, and faster than noncontact printers (15). Contact printing has been used to pattern biomaterials, including DNA (16, 17), colloidal crystal arrays (18), and monoclonal antibodies (19), where elements can be densely packed in spatially defined areas. Recently several new types of contacting printing have emerged including dip pen nanolithography (DPN) (20) and varied forms of printing based on a PDMS continuous flow microf-

* To whom correspondence should be addressed. Tel: (951) 827-2702. Email: quan.cheng@ucr.edu. Fax: (951) 827-4713.
Received for review April 29, 2009 and accepted June 30, 2009
[†] University of California, Riverside.
[‡] University of California, Davis.
DOI: 10.1021/am900290g

luidic device (21). In spite of good flow control and small sample volume, one major drawback of patterning using microfluidics is that elaborate patterns with features more complex than simple cross patterned strips, such as arrays in high density, are hard to achieve without additional fabrication steps (22). The most popular method of contact printing employed currently is still the use of solid pins. There are a number of advantages to this technology including easy deposition of viscous solutions (23), simple design that enables reproducible and efficient printing (24), and simple cleaning procedure for the pins (24). One unique variant to the solid pin design is the pin and ring spotter employed in the GMS 417 arrayer, which uses a large ring to hold the sample and the pass of a pin deposits a droplet (25). The coefficient of variation (CV) using the GMS 417 Arrayer has been reported to be <10% previously (26), and several groups have used the device to examine a multitude of biological interactions including arrays of antibodies (27), extracellular matrix proteins (ECM) (28), tissue lysates (29), as well as organic dyes and ionic substances (30). Despite the widespread application of contact printers, in-depth examination of morphological features of the printed elements created by contact printing and their dependence on surface chemistry is generally lacking.

Biomolecular interaction studies desire proper orientation of the ligands and probe density for functional binding. It is known that surface chemistry employed to immobilize the biomolecules of choice is of great importance. This is especially true when immobilizing carbohydrates in an array format. Among various covalent coupling approaches that are typically used, one main problem is the lack of control with regards to the orientation of the probe glycan relative to the surface (8). In addition, how this lack of control affects detection performance with new detection schemes such as label-free methods has not been investigated as the majority of detection is fluorescence-based. Label-free detection with microarray has gained considerable acceptance in the past few years (31, 32), and there was a recent report that uses SPR and XPS to examine a self-assembled carbohydrate monolayer for array analysis (33). But in general, the effects of carbohydrate immobilization on microarray performance and reliability, especially that involving protein-based surface chemistries, has not been extensively studied.

We report here the fabrication of a carbohydrate microarray using contact printing with biotinylated sialosides and the characterization of the array morphology with a series of surface microscopic techniques. The array has been further characterized for its effectiveness in the study of interactions with lectins by surface plasmon resonance imaging (SPRi). SPR imaging allows multiplex detection of biological interactions with real-time kinetic analysis possible (34). We recently demonstrated an SPR spectroscopic analysis with surface chemistry based on synthetic sialosides for the detection of lectins (35). The leap to microarray and imaging analysis will enable multiplexed examination of carbohydrates in their native state and yield desirable affinity information with speed. There are a few attempts recently that aim to combine SPR with array analysis (36–38), including a carbohydrate microarray that was created by electropolymerization in a 25 spot matrix for the detection of proteins (36). In this work, a home-built SPR imaging system (39) is utilized along with a commercial contact printing arrayer (the pin-and-ring arrayer) to reveal the morphological connection to biotin–neutravidin chemistry in the immobilization of carbohydrates and its impact on performance. The arrayer is employed to create upward of 400 individual array elements for demonstrating proof of principle for high density fabrication with quality. In addition, regeneration of the surface is investigated, which aims to substantially reduce material cost and time associated with sample preparation and measurement. We also compare biotin–avidin surface chemistry attachment to covalent attachment of protein analytes and examine their effects on fabrication reproducibility and binding efficiency. The biointerface design described herein should be applicable to many biological systems for high throughput bioanalysis.

EXPERIMENTAL SECTION

Materials. *Sambucus nigra* agglutinin (SNA) and fluorescein tagged-SNA (FL-SNA) were purchased from Vector Laboratories (Burlingame, CA). Biotinylated bovine serum albumin (b-BSA), neutravidin, avidin, and streptavidin were purchased from Pierce Biotechnology (Rockford, IL). Bovine serum albumin (BSA), 11-mercaptoundecanoic acid (MUA), N-hydroxysuccinimide (NHS), 1-(3-Dimethylaminopropyl)-3-ethylcarbodiimide hydrochloride (EDC), cholera toxin (CT) from *Vibrio cholerae*, and anticholera toxin from rabbit (anti-CT) were obtained from Sigma-Aldrich (St. Louis, MO). SPR gold chips with a 2 nm chromium adhesion layer and 46 nm of gold were deposited by e-beam evaporation onto cleaned BK-7 glass slides and were subsequently used in all assays. All SPR and SPR imaging experiments used a 20 mM phosphate buffered saline (pH 7.4 with 150 mM NaCl) as both a running buffer and dilution buffer. All biotinylated sialosides were synthesized as previously described (35).

Carbohydrate Array Fabrication and SPR Imaging. The substrate for the arrays was generated by depositing 0.5 mg/mL biotin-BSA onto a gold SPR substrate and allowing incubation on a shaker in a humid environment for 30 min. Then the surface was copiously rinsed with DI water to avoid salt buildup from the buffer; 0.5 mg/mL neutravidin was added to the substrate, followed by incubation and rinsing as previously mentioned. The sensor chip was then placed in the GMS 417 Arrayer for printing of 20 × 20 arrays of four different biotinylated carbohydrates and BSA control. Smaller sets of 2 × 2 arrays containing the same compounds were fabricated as well for comparison experiments. The GMS 417 Arrayer uses the pin-and-ring type of contact printing technology, which delivers highly reproducible dots (40). The arrayed spots were approximately 150 μm in diameter and spot spacing (center-to-center) was adjusted from 300–375 μm.

After creation of the carbohydrate microarrays, the arrays were imaged on a home-built SPR imager, which has been described previously (39). Thereafter, 500 μg/mL SNA (or fluorescein-tagged SNA) was deposited on the substrate, and the arrays were imaged once again. The image before SNA binding was subtracted from the image after binding to obtain difference images, with data analyzed in a similar manner to our previous publications (41, 42). For confirmation of binding events, FL-SNA was deposited on the carbohydrate functionalized surface and images of the arrayed substrate were obtained with a confocal fluorescence microscope.

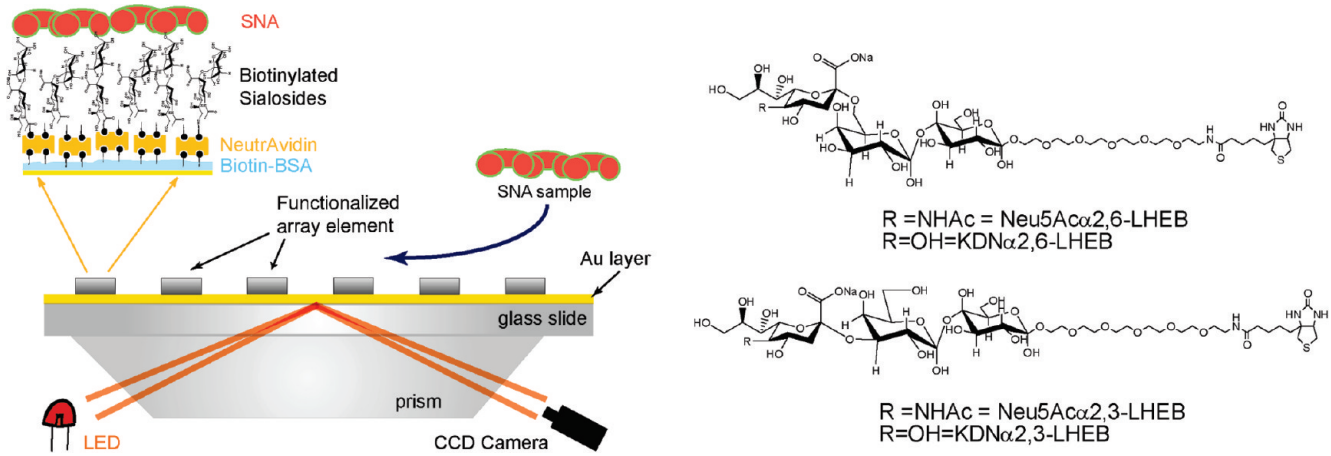

FIGURE 1. Schematic of the carbohydrate microarray surface chemistry and the structures of the four biotinylated sialosides.

Covalent Fabrication of Protein Microarray. The gold SPR substrates were immersed in 1 mM MUA for overnight incubation. Thereafter the chips were rinsed and dried in N_2, and EDC/NHS (4:1 molar ratio) was added to the surface to generate reactive NHS ester to facilitate the formation of a stable intermediate for subsequent protein immobilization (43). After a short incubation and rinsing step, anti-CT (1.0 mg/mL) was arrayed on the active surface by the GMS 417 arrayer. Then CT (200 μg/mL) was deposited across the surface, and the chip was rinsed extensively before its use for analysis.

Atomic Force Microscopy (AFM) Characterization of Array Substrates. AFM images were obtained using a Veeco Dimension 5000 atomic force microscope (Santa Barbara, CA) with manufacturer provided software. Arrays were identified with the AFM microscope by using alignment marks on the substrate, and from there, images from among arrays, on the edge of array elements, and between arrays were taken. All images were obtained under the tapping mode and root-mean-square (rms) surface roughness values were obtained by averaging multiple 225 μm^2 areas across the entire imaged substrate at a scan rate of 1 Hz.

Fluorescence Microscopic Analysis of Carbohydrate Microarrays. Fluorescence microscopy experiments were carried out on a Zeiss LSM 510 confocal laser scanning microscope (CLSM) with 488 nm argon laser excitation, CCD camera, and 527 nm long pass emission filter with a 10x objective. The carbohydrate arrays were fabricated in the same manner as normal SNA arrays as noted above. After FL-SNA was deposited, the surface was incubated and rinsed. The substrate was placed in a Petri dish and covered with aluminum foil until analysis to avoid photodegradation. Snapshot fluorescent images were taken of the arrayed substrates and presented without further optimization.

RESULTS AND DISCUSSION

SPR Imaging Analysis of Carbohydrate Microarray. A scheme of the biointerface examined in this work is shown in Figure 1 with individual element details. Also depicted in Figure 1 are the structures of the biotinylated sialosides used for building the arrays and their synthesis can be found in a previous publication (7). The substrate was treated with biotin-BSA, followed by addition of neutravidin. These steps served two important purposes: to build up the surface chemistry for the arraying process and to passivate the surface to suppress nonspecific adsorption. The surface coverage of the biotin-BSA layer can be calculated from SPR results to determine the efficiency of immobilization and thus explain the strong coupling efficiency with the subsequent neutravidin sublayer. To assess the amount of adsorbed protein, methods from Jung et al. were applied (44). The adsorbate film thickness is determined by the following (eq 1) (44):

$$d = -(l_d/2)\ln(1 - R/R_{max}) \quad (1)$$

where d is the adsorbate film thickness, l_d is the decay length, which can be estimated at 37% of the wavelength of light (670 nm), so in this case l_d is 247.9 nm, R is the response in degrees, and R_{max} is the maximum response that would be measured for an infinitely thick adlayer or

$$R_{max} = m(\eta_a - \eta_s) \quad (2)$$

where m is the sensitivity factor of the instrument estimated at 100 deg/RIU, η_a is the biotin-BSA refractive index estimated at 1.57 (44), and η_s is PBS buffer refractive index measured to be 1.340 with an Abbe refractometer. Plugging in the known values in eq 1 and using the specific volume of biotin-BSA (0.77 cm^3/g) (45), the surface coverage of biotin-BSA is determined to be 1.32×10^{-7} g/cm^2. This value is very close to the reported surface coverage of serum albumin proteins adsorbed on gold under similar conditions (46).

In addition, the orientation of the adsorbed protein is estimated to account for the efficient establishment of the neutravidin layer. Two different arrangements of the ellipsoidal-shaped BSA on a substrate are possible: a parallel (or side-on type) and a perpendicular (or end-on type) orientation. If the gold substrate is covered with a monomolecular layer of BSA the parallel orientation surface coverage should be close to 140 ng/cm^2 (47, 48). The biotin-BSA surface employed here yields a 132 ng/cm^2 surface coverage, confirming a parallel orientation of the biotin-BSA on gold, as similarly observed with other studies (49, 50). This high-density, parallel orientation of the biotin-BSA layer apparently allows for a reproducible and strong binding of neutravidin to functionalize the substrate. Thereafter 20 ×

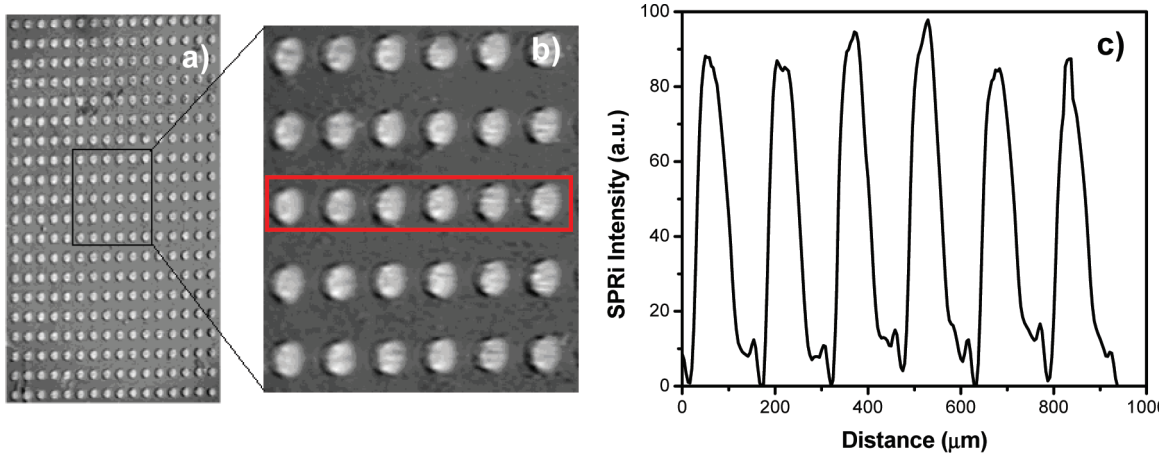

FIGURE 2. SPR difference image of a high density carbohydrate microarray of (a) Neu5Aca2,6-LHEB interacting with 500 μg/mL SNA, (b) a zoomed up SPR image of a 6 × 5 arrayed area, and (c) the corresponding reflection intensity profile for the array elements.

20 arrays of four different biotinylated carbohydrates were deposited with a contact arrayer and the chips were then imaged with an SPR imager. Difference images for the Neu5Acα2,6-LHEB functionalized array are shown in Figure 2. The difference images were obtained by subtracting the image before SNA binding from the image after binding, with data analyzed in a similar manner to that in our previous publication (12). The high reflection intensity in Figure 2a and b clearly shows the binding of SNA to the carbohydrate array made by Neu5Acα2,6-LHEB. SNA specifically binds to α2,6-linked sialosides well (51), so this result is expected. The blown up image in Figure 2b along with its corresponding profile in Figure 2c readily demonstrates the high reproducibility of the array and low nonspecific adsorption. The coefficient of variance (CV) of the array before SNA deposition was determined to be 3.2% by using the SPRi reflection intensity (RI). After SNA binding, the CV increased slightly to 4.3%, which still places this microarray on par or better than most other microarrays reported in literature. The high specificity of binding interaction and minimal array element-to-element variation make this carbohydrate microarray scheme very useful to monitor protein-carbohydrate interactions. Furthermore, addition of 100 mM glycine, pH 1.7 to the chip surface removes the lectin entirely while leaving the carbohydrate intact and functional (data not shown). This property allows the generation of a fresh carbohydrate surface for reuse of the array in subsequent binding experiments. The CV of the array after stripping buffer treatment is 8.2%, showing the effectiveness of the stripping process.

Multiplexed SPR imaging analysis of lectin-carbohydrate interactions were also performed and the results are shown in Figure 3. Each image depicted in Figure 3 is a 2 × 2 carbohydrate array after deposition of 500 μg/mL SNA. In addition, a BSA control array was fabricated for comparison, and reflection intensities for the four biotinylated sialosides and control are listed as well. It is important to note that all carbohydrates and BSA were deposited as clusters of arrays on the same substrate and therefore subjected to the same experimental conditions. The strongest binding signal is obtained for the Neu5Acα2,6-LHEB (RI = 128.2 au), which

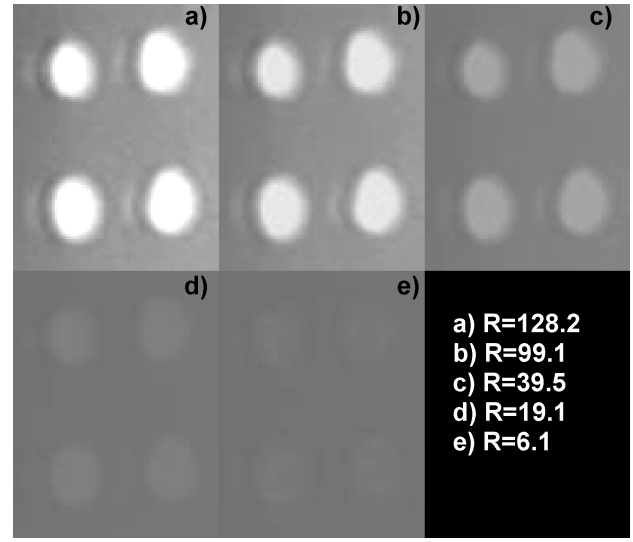

FIGURE 3. SPR images of 2 × 2 arrayed spots upon interaction with 500 μg/mL SNA for chips immobilized with (a) Neu5Acα2,6-LHEB, (b) KDNα2,6-LHEB, (c) Neu5Acα2,3-LHEB, (d) KDNα2,6-LHEB, and (e) BSA. The reflection intensity for each image is noted in the bottom right position of the figure.

is known to have high affinity to SNA. This is followed by the KDNα2,6-LHEB, which has an RI of 99.1. The binding interaction for this sialoside is weaker than that for Neu5Acα2,6-LHEB as the difference here in carbohydrate structure is a missing *N*-acetyl at the C5 carbon of sialic acid, which is replaced with a hydroxyl moiety. There is a large drop-off in binding observed for the Neu5Acα2,3-LHEB (RI = 39.5 au), illustrating the importance of sialyl linkage on binding affinity, which has been previously documented (40, 52). Finally the weakest binding biotinylated sialoside in this group is the KDNα2,6-LHEB with an RI of 19.1. This carbohydrate has both a different sialyl linkage and a different functional group on sialic acid, largely altering the structural moiety necessary for maximum binding. This relative binding interaction pattern agrees quite well with previous SPR spectroscopic studies by our group (35), indicating the successful creation and application of a carbohydrate microarray. In the control, the interaction of bovine serum albumin (BSA) with SNA was tested for nonspecific binding

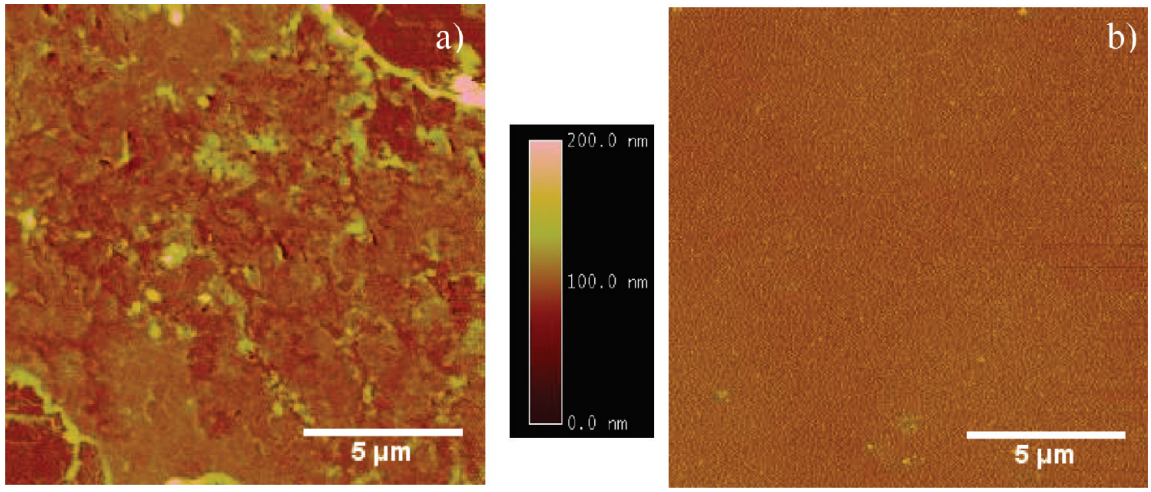

FIGURE 4. AFM image of (a) the Neu5Acα2,6-LHEB based array element after SNA interaction and (b) the space in between array elements.

and only a small signal (6.1 a.u) was obtained, suggesting that the SNA-carbohydrate interactions are highly specific. Clearly the results reported here show that this carbohydrate microarray is able to distinguish small variations in carbohydrate structure and their effect on binding in a quantitative manner.

Effect of Avidin Proteins on Array Measurement. An important goal of this work is to explicitly determine any potential correlation between structural/morphological characteristics of the printed elements and performance and seek to maximize analytical merits through optimized conditions and unique interfacial design. Use of different avidin proteins for immobilization of biotinylated sialosides was thus investigated. SPR spectroscopy was first used to examine three major classes of avidin proteins: avidin, streptavidin, and neutravidin. Avidin is a glycoprotein containing four identical subunits with a combined molecular mass of ~67 kD. It consists of 128 amino acids and has an isoelectric point of 10−10.5. Chemical modification has little effect on the activity of avidin, and it is stable over a wide range of pH values and temperatures. Streptavidin is a 53kD nonglycosylated avidin protein with a lower isoelectric point (6.8−7.5) and tends to have low nonspecific binding. Neutravidin contains no carbohydrate and has a near-neutral isoelectric point (6.3), providing a useful agent with very low nonspecific binding (lower than streptavidin) and broader utility in a variety of applications (53, 54). For the biointerfaces tested here, these features of neutravidin make it highly desirable for protein−sugar interactions. SPR spectroscopic data indicated that at saturation levels of lectin the change in minimum angle for nonspecific avidin binding was largest (62.2 ± 5.1 mdeg), while for streptavidin, the nonspecific binding signal was considerably lower (37.1 ± 4.2 mdeg). The lowest nonspecific binding was observed for neutravidin as expected (24.9 ± 3.1 mdeg), roughly two-thirds that of streptavidin and only 40% of avidin. Furthermore, SPR binding analysis reveals that on Neu5Acα2,6-LHEB biotinylated sialoside surface SNA has the strongest binding signal (background corrected) with a neutravidin protein sublayer. Given the deglycosylation nature of neutravidin the overwhelming majority of binding occurs between the lectin (SNA) and the carbohydrate, not the protein sublayer and carbohydrate. In contrast, avidin tends to bind both the carbohydrate and the lectin thus resulting in a generally weaker signal for specific SNA/carbohydrate interactions. For streptavidin, the specific signal is larger than for avidin, but given the higher pI compared to neutravidin, some electrostatic interactions with the protein sublayer is most likely responsible for the smaller specific binding compared to neutravidin. Therefore carbohydrate microarrays prepared with a neutravidin protein sublayer demonstrate better signal performance as compared to other protein sublayers, making this sublayer a desirable surface for carbohydrate microarray fabrication.

AFM Characterization of Carbohydrate Microarrays. AFM was employed to characterize the morphological features of the arrays and to verify if a specific binding interaction was taking place on the surface of the carbohydrate microarray elements. AFM has been effectively used to examine molecular orientation as well as surface roughness and height distributions (55). The image shown in Figure 4a is the center of an array element on the Neu5Acα2,6-LHEB functionalized microarray with SNA deposited. This image clearly indicates the buildup of materials in the array element, and the surface roughness has increased to 10.5 ± 0.8 nm. In comparison, the surface roughness measured between array elements on the same microarray (Figure 4b) was much smaller (only 2.8 ± 0.2 nm). The roughness value for the Neu5Acα2,6-LHEB functionalized array element without SNA interaction was 5.6 ± 0.5 nm. These numbers clearly show that the buildup of material in the array element originates from SNA binding to the probe carbohydrate immobilized in the array element. Similar experiments have been performed on other functionalized carbohydrate microarrays before and after SNA deposition, and the surface roughness values are given in Table 1. Interestingly, the Neu5Acα2,6-LHEB functionalized microarray shows the largest difference in surface roughness before and after protein binding, and surface roughness differences appear to decrease with decreasing affinity. The relative binding

Table 1. AFM Surface Roughness on the Carbohydrate Functionalized Array Elements before and after Deposition of 500 μg/mL SNA

carbohydrate	surface roughness (nm), carbohydrate	surface roughness (nm) with SNA
Neu5Acα2,6-LHEB	5.6 ± 0.5	10.5 ± 0.8
KDNα2,6-LHEB	5.2 ± 0.3	7.5 ± 0.7
Neu5Acα2,3-LHEB	5.7 ± 0.3	5.9 ± 0.4
KDNα2,3-LHEB	5.6 ± 0.2	5.8 ± 0.4

between the four carbohydrates obtained from the roughness measurements was very similar to that observed with the SPR imaging data. It offers an alternative to quantify affinity on a surface and provides supporting evidence of carbohydrate functionalization and subsequent protein binding by SNA.

Fluorescence Microscopic Analysis of FL-SNA Binding to Microarrays. AFM is highly useful for topological characterization but fails to provide chemical information about the array and the binding events on the array elements. Fluorescence microscopy was thus used to further confirm specific carbohydrate–protein interactions. Figure 5 is a 2 × 2 fluorescent array snapshot for the Neu5Acα2,6-LHEB functionalized microarray interacting with FL-SNA. The concentration of fluorescein-SNA was the same as SNA (500 μg/mL) used in the SPRi experiments. The fluorescence signal is much brighter in the array elements than in the surrounding areas, which confirms that a specific binding event between SNA and the carbohydrate takes place on the surface. It is worth noting that there is a faint fluorescence background throughout the array. In a control experiment using only fluorescein dye on the carbohydrate microarray, a faint fluorescence signal was also observed from minimal nonspecific binding to the neutravidin layer. Thus the well-defined neutravidin-laden sublayer ideal for label-free SPR imaging analysis may contribute to certain degree of background fluorescence if a conventional fluorescence measurement is employed.

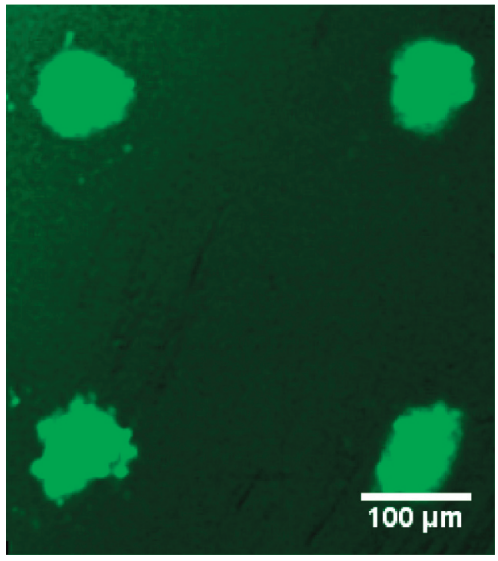

FIGURE 5. Fluorescence image of Neu5Acα2,6-LHEB array with SNA interaction on the surface.

Biointerface Comparison: Biotin–Avidin Chemistry versus Covalent Coupling. As a comparison to demonstrate the advantage of biotin–neutravidin chemistry for interface construction, a microarray using covalent attachment was also fabricated. This covalent array immobilized anticholera toxin (anti-CT) for detection of bacterial cholera toxin (CT). The array was fabricated on an activated SAM surface in a similar manner as the carbohydrate microarrays previously discussed except in this case an antibody, anti-CT, was printed. For the carbohydrate interface it is imperative to not disrupt the structure, while exposing the functional sites so native carbohydrate–protein interactions can take place (56). Carbohydrates do not have functional groups for orientation, so it is often difficult to immobilize them in an oriented and functional fashion (9, 57). Designing an interface based on the biotin–neutravidin interaction seems inherently important in our carbohydrate microarray for proper orientation of the glycan probe for subsequent protein binding. The covalent coupling, on the other hand, is very routinely used when immobilizing a probe like a protein. However, studies indicate that the use of covalent coupling can often result in the random orientation of probe species and the denaturation/change in inherent chemical structure, which can affect the efficacy of binding to other biomolecules (58). This is because there are a number of possible orientations that the modified biomolecule may adopt on the substrate surface through the use of a SAM (59). From an experimental standpoint for any microarray, if probe orientation is compromised, there should be poor uniformity in the binding pattern of the analyte along with nonspecific protein adsorption. To test this assumption 200 μg/mL CT was applied on the anti-CT functionalized array surface and the respective SPR difference image and binding profile (outlined by a red rectangle) are displayed in Figures 6. As is evident from the SPR image in Figure 6, there is a large degree of inhomogeneity on the array elements despite the well-characterized strong interaction between anti-CT and CT ($K_a = 1.4 \times 10^9$ M^{-1}) (60). In fact, the SPR imaging data suggests that on most of the array elements there is a surface buildup on the edge of the array elements themselves rather than dispersed throughout the element indicating a possible probe immobilization and orientation inhomogeneity. Quantitatively this is described by the CV of the row of array elements indicated in Figure 6b at ~16% or three times the value of the biotin–neutravidin based carbohydrate microarray. This substantial signal variation is not conducive for high-confidence quantitative measurements in an array format. These data indicate the covalent method of probe immobilization is not ideal if orientation and structural integrity of the probe molecule must be highly preserved, which is achievable with a biotin–neutravidin-based interface. A similar conclusion has been previously reported where the authors determined a biotin–streptavidin-based surface system more reliable than a NHS-modified SAM in examining antibody–antigen interactions with fluorescence and other surface analytical techniques (61).

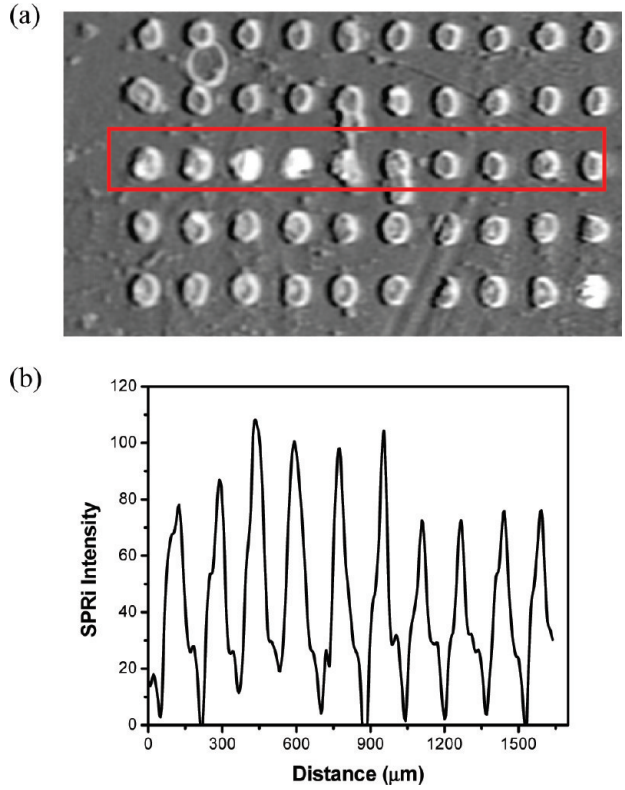

FIGURE 6. SPR image of (a) anti-CT/CT array and (b) the corresponding line profile as outlined by the red rectangle in the SPR image in a.

To further determine the morphological characteristics of specific interaction occurring on the anti-CT array elements, AFM images were collected and results are shown in Figure 7. Inside an individual array element there is minimal binding demonstrated (Figure 7a). The surface roughness values are not very high in the array element itself and there are large deviations even within the array element (rms = 11 ± 6.2 nm). This surface roughness value is only about 1 nm higher than the anti-CT microarray elements without CT. The large standard deviation in array element roughness also confirms what was observed optically with SPR imaging, which exhibited lack of uniform binding. Figure 7b shows the surface between array spots demonstrating similar roughness as that of an array element (10.5 ± 6.8 nm), indicating a high degree of nonspecific adsorption. Finally, the buildup of binding material on the edge of individual array elements observed on the SPR images is confirmed with AFM as shown in Figure 7c. While on the edge of the individual array element there is obvious surface buildup (rms = 24 ± 1.5 nm) the rest of the array element in the same image (rms = 10 ± 5.5 nm) is not nearly as rough. This nonuniformity that was observed throughout the anti-CT array provides substantial evidence that probe immobilization orientation cannot be achieved effectively with NHS-modified SAMs. The biotinylation process reported here can be adapted for use to orient nearly any biomolecule on many substrates. We have recently demonstrated the use of nanoscale thick glass on gold for nonlabeling SPR and SPR imaging examination of various biointeractions (62, 63). Future work will be focused on obtaining kinetic data from the SPR imaging experiments and combining the biotinylated interface with new substrates for various biosensing applications involving proteins, carbohydrate, and other biomolecules.

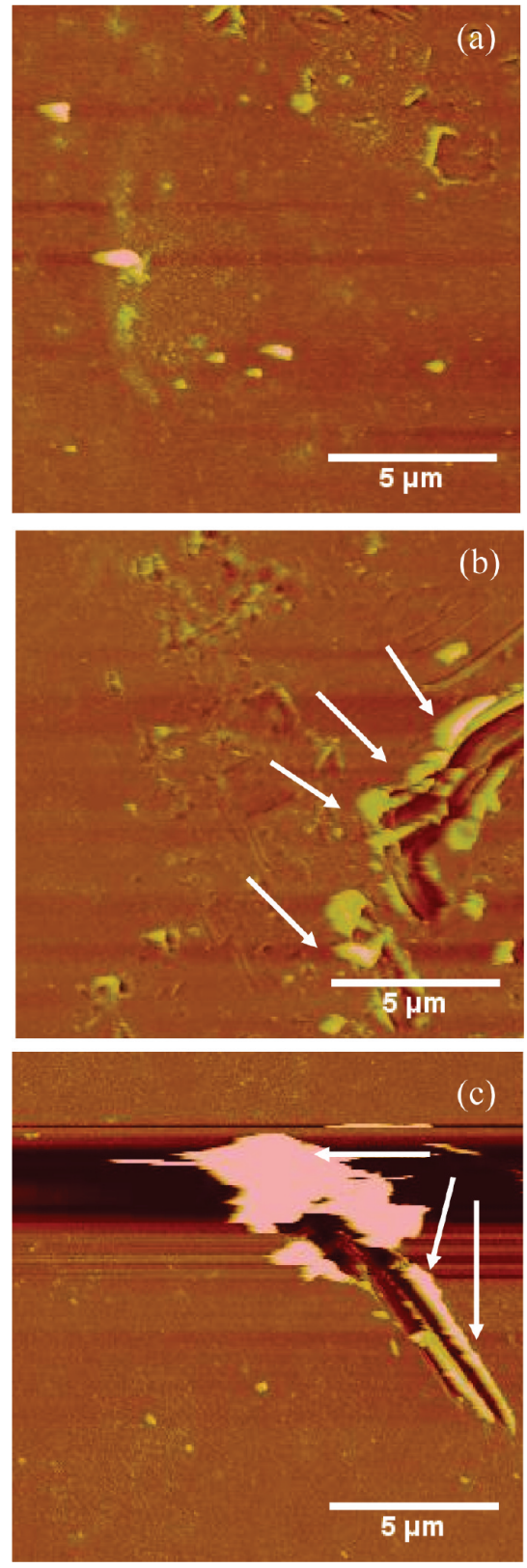

FIGURE 7. AFM images of the anti-CT array as shown in Figure 6. (a) The center area of an anti-CT array spot (inside the array element), (b) space between the array spots, and (c) on the edge of an array spot after CT interaction with white arrows indicating the edge of the array element for both b and c.

CONCLUSIONS

The results reported in this study demonstrate reusable carbohydrate microarrays employing contact printing and interface design with biotinylated sialosides and biotin−neutravidin interactions. The properties of this biointerface have been investigated extensively by SPR, SPR imaging, AFM, and fluorescence microscopy to demonstrate the advantageous nature of the design. In comparison with the covalent microarray of anti-CT, the carbohydrate microarray based on biotin−neutravidin chemistry provides three times lower CV values, a much more homogeneous array, and very little nonspecific adsorption. All of these factors make the reported microarray biointerface highly attractive and suited for study of not only carbohydrate−protein interactions but also protein−protein and other biomolecule−protein interactions in a high-throughput manner. In comparison to a NHS-modified SAM, which is primarily used for fluorescence detection, the biotin−neutravidin biointerface can be applied to both labeled and label-free detection schemes, which largely expands the choice of detection platforms when switching to more advantageous label-free analysis.

Acknowledgment. The authors would like to acknowledge financial support from NSF grant CHE-0719224.

REFERENCES AND NOTES

(1) Hakomori, S. *Glycoconj. J.* **2004**, *21*, 125–137.
(2) Housman, B. T.; Mrksich, M. *Chem. Biol.* **2002**, *9*, 443–454.
(3) Park, S.; Shin, I. *Angew. Chem., Int. Ed.* **2002**, *41*, 3180–3182.
(4) Wang, D.; Liu, S.; Trummer, B. J.; Deng, C.; Wang, A. *Nat. Biotechnol.* **2002**, *20*, 275–281.
(5) Fukui, S.; Feizi, T.; Galustian, C.; Lawson, A. M.; Chai, W. *Nat. Biotechnol.* **2002**, *20*, 1011–1017.
(6) Horlacher, T.; Seeberger, P. H. *Chem. Soc. Rev.* **2008**, *37*, 1414–1422.
(7) Horlacher, T.; Seeberger, P. H. *OMICS* **2006**, *10*, 490–498.
(8) Liang, P.-H.; Wu, C.-Y.; Greenberg, W. A.; Wong, C.-H. *Curr. Opin. Chem. Biol.* **2008**, *12*, 86–92.
(9) De Paz, J. L.; Seeberger, P. H. *QSAR Comb. Sci.* **2006**, *25*, 1027–1032.
(10) Culf, A. S.; Cuperlovic-Culf, M.; Ouellette, R. J. *OMICS* **2006**, *10*, 289–310.
(11) Park, S.; Lee, M.-R.; Shin, I. *Chem. Commun.* **2008**, 4389–4399.
(12) Dulcey, C. S.; Georger, J. H.; Krauthamer, V.; Stenger, D. A.; Fare, T. L.; Calvert, J. M. *Science* **1991**, *252*, 551–554.
(13) Allain, L. R.; Stratis-Cullum, D. N.; Vo-Dinh, T. *Anal. Chim. Acta* **2004**, *518*, 77–85.
(14) Tseng, F. G.; Kim, C. J.; Ho, C. M. *J. Microelectromech. S.* **2002**, *11*, 427–436.
(15) Walther, M.; Stillman, B.; Fribe, A.; Beator, J. http://www.whatman.com/, 2007, pp 7−8.
(16) Rose, D. In *Microarray Biochip Technology*; Schena, M., Ed.; Eaton Publishing: Natick, MA, 2000, pp 19−38.
(17) Clark, S. M.; Harnilton, G. E.; Nordmeyer, R. A.; Uber, D.; Cornell, E. W.; Brown, N.; Segraves, R.; Davis, R.; Albertson, D. G.; Pinkel, D. *Anal. Chem.* **2008**, *80*, 7639–7642.
(18) Burkert, K.; Neumann, T.; Wang, J. J.; Jonas, U.; Knoll, W.; Ottleben, H. *Langmuir* **2007**, *23*, 3478–3484.
(19) Rieger, M.; Cervino, C.; Sauceda, J. C.; Niessner, R.; Knopp, D. *Anal. Chem.* **2009**, *81*, 2373–2377.
(20) Piner, R. D.; Zhu, J.; Xu, F.; Hong, S. H.; Mirkin, C. A. *Science* **1999**, *283*, 661–663.
(21) Natarajan, S.; Hatch, A.; Myszka, D. G.; Gale, B. K. *Anal. Chem.* **2008**, *80*, 8561–8567.
(22) Ruiz, S. A.; Chen, C. S. *Soft Matter* **2007**, *3*, 168–177.
(23) Weibel, C. *J. Assoc. Lab. Automation* **2002**, *7*, 91–96.
(24) Barbulovic-Nad, I.; Lucente, M.; Sun, Y.; Zhang, M. J.; Wheeler, A. R.; Bussmann, M. *Crit. Rev. Biotechnol.* **2006**, *26*, 237–259.
(25) Mace, M. L.; Montagu, J.; Rose, S. D.; Mcguinness, G. In *Microarray Biochip Technology*; Eaton Publishing: Natick, MA, 2000, pp 39−64.
(26) Müller, U. R.; Papen, R. In *Microarray Technology and Its Applications*; Müller, U. R., Nicolau, D. V., Eds.; Springer: Berlin, 2005, pp73−77.
(27) Stybayeva, G.; Zhu, H.; Ramanculov, E.; Dandekar, S.; George, M.; Revzin, A. *Biochem. Bioph. Res. Co.* **2009**, *380*, 575–580.
(28) Lee, J. Y.; Shah, S. S.; Zimmer, C. C.; Liu, G. Y.; Revzin, A. *Langmuir* **2008**, *24*, 2232–2239.
(29) Nishizuka, S.; Charboneau, L.; Young, L.; Major, S.; Reinhold, W. C.; Waltham, M.; Kouros-Mehr, H.; Bussey, K. J.; Lee, J. K.; Espina, V.; Munson, P. J.; Petricoin, E.; Liotta, L. A.; Weinstein, J. N. *Proc. Natl. Acad. Sci. U. S. A.* **2003**, *100*, 14229–14234.
(30) Andreeva, L. V.; Koshkin, A. V.; Letiedev-Stepanov, P. V.; Petrov, A. N.; Alfimov, M. V. *Colloid Surface A* **2007**, *300*, 300–306.
(31) Lausted, C.; Hu, Z. Y.; Hood, L. *Mol. Cell. Proteomics* **2008**, *7*, 2464–2474.
(32) Seidel, M.; Niessner, R. *Anal. Bioanal. Chem.* **2008**, *391*, 1521–1544.
(33) Dhayal, M.; Ratner, D. M. *Langmuir* **2009**, *25*, 2181–2187.
(34) Chen, Y. L.; Nguyen, A.; Niu, L. F.; Corn, R. M. *Langmuir* **2009**, *25*, 5054–5060.
(35) Linman, M. J.; Taylor, J. D.; Yu, H.; Chen, X.; Cheng, Q. *Anal. Chem.* **2008**, *80*, 4007–4013.
(36) Mercey, E.; Sadir, R.; Maillart, E.; Roget, A.; Baleux, F.; Lortat-Jacob, H.; Livache, T. *Anal. Chem.* **2008**, *80*, 3476–3482.
(37) Karamanska, R.; Clarke, J.; Blixt, O.; Macrae, J. I.; Zhang, J. Q.; Crocker, P. R.; Laurent, N.; Wright, A.; Flitsch, S. L.; Russell, D. A.; Field, R. A. *Glycoconj. J.* **2008**, *25*, 69–74.
(38) Liu, W.; Chen, Y.; Yan, M. *Analyst* **2008**, *133*, 1268–1273.
(39) Wilkop, T.; Wang, Z.; Cheng, Q. *Langmuir* **2004**, *20*, 11141–11148.
(40) Duverger, E.; Coppin, A.; Strecker, G.; Monsigny, M. *Glycoconj. J.* **1999**, *16*, 793–800.
(41) Taylor, J. D.; Linman, M. J.; Wilkop, T.; Cheng, Q. *Anal. Chem.* **2009**, *81*, 1146–1153.
(42) Wang, Z.; Wilkop, T.; Han, J.-H.; Dong, Y.; Linman, M. J.; Cheng, Q. *Anal. Chem.* **2008**, *80*, 6397–6404.
(43) Geng, P.; Zhang, X. N.; Meng, W. W.; Wang, Q. J.; Zhang, W.; Jin, L. T.; Feng, Z.; Wu, Z. R. *Electrochim. Acta* **2008**, *53*, 4663–4668.
(44) Jung, L. S.; Campbell, C. T.; Chinowsky, T. M.; Mar, M. N.; Yee, S. S. *Langmuir* **1998**, *14*, 5636–5648.
(45) Sjolander, S.; Urbaniczky, C. *Anal. Chem.* **1991**, *63*, 2338–2345.
(46) Fair, B. D.; Jamieson, A. M. *J. Colloid Interface Sci.* **1980**, *77*, 525–534.
(47) Zhang, Y.; Meiling, W.; Qingji, X.; Xianhui, W.; Shouzhuo, Y. *Sensor Actuat. B, Chem.* **2005**, *105*, 454–463.
(48) Aung, K. M. M.; Ho, X. N.; Su, X. D. *Sensor Actuat. B, Chem.* **2008**, *131*, 371–378.
(49) Kim, N. H.; Baek, T. J.; Park, H. G.; Seong, G. H. *Anal. Sci.* **2007**, *23*, 177–181.
(50) Whelan, R. J.; Zare, R. N. *Anal. Chem.* **2003**, *75*, 1542–1547.
(51) Shibuya, N.; G, I. J.; Broekaert, W. F.; Nsimba-Lubaki, M.; Peeters, B.; Peumans, W. J. *J. Biol. Chem.* **1987**, *262*, 1596–1601.
(52) Knibbs, R. N.; Goldstein, I. J.; Ratcliffe, R. M.; Shibuya, N. *J. Biol. Chem.* **1991**, *266*, 83–88.
(53) Hiller, Y.; Gershoni, J. M.; Bayer, E. A.; Wilchek, M *Biochem. J.* **1987**, *248*, 167–171.
(54) Kheirolomoom, A.; Dayton, P. A.; Lum, A. F. H.; Little, E.; Paoli, E. E.; Zheng, H.; Ferrara, K. W. *J. Controlled Release* **2007**, *118*, 275–284.
(55) Chen, S.; Liu, L.; Zhou, J.; Jiang, S. *Langmuir* **2003**, *19*, 2859–2864.
(56) Seo, J. H.; Adachi, K.; Lee, B. K.; Kang, D. G.; Kim, Y. K.; Kim, K. R.; Lee, H. Y.; Kawai, T.; Cha, H. J. *Bioconjugate Chem.* **2007**, *18*, 2197–2201.
(57) Shin, I.; Park, S.; Lee, M.-R. *Chem.—Eur. J.* **2005**, *11*, 2894–2901.
(58) Saerens, D.; Huang, L.; Bonroy, K.; Muyldermans, S. *Sensors* **2008**, *8*, 4669–4686.
(59) Ferretti, S.; Paynter, S.; Russell, D. A.; Sapsford, K. E.; Richardson, D. J. *Trends Anal. Chem.* **2000**, *19*, 530–540.
(60) Labib, M.; Hedstrom, M.; Amin, M.; Mattiasson, B. *Anal. Chim. Acta* **2009**, *634*, 255–261.
(61) Schaferling, M.; Riepl, M.; Pavlickova, P.; Paul, H.; Kambhampati, D.; Liedberg, B. *Microchim. Acta* **2003**, *142*, 193–203.
(62) Phillips, K. S.; Han, J.-H.; Martinez, M.; Wang, Z.; Carter, D.; Cheng, Q. *Anal. Chem.* **2006**, *78*, 596–603.
(63) Linman, M. J.; Culver, S. P.; Cheng, Q. *Langmuir* **2009**, *25*, 3075–3082.

AM900290G